Journal of Applied Sciences and Modelling

https://journal.krrishpub.com/index.php/jasm/index

# A Comprehensive Review of Electrostatic Modelling in Biomolecular Simulations

Adari Sasi Sahasra[a], Abdul Kowsar[a], Arnab Mukherjee [b], Suman Saurabh [c,*]

[a] *Department of Electrical Engineering, National Institute of Technology Andhra Pradesh, Tadepalligudem, 534101, India.*
[b] *Department of Drug Discovery, Qubit Pharmaceuticals, 201 Rue Lecourbe, Paris, 75015, France.*
[c] *School of Sciences, National Institute of Technology Andhra Pradesh,Tadepalligudem, 534101, India.*

**Abstract**

Electrostatic interactions are omnipresent in biology and play an important role in carrying out and determining the outcome of biological processes. Understanding biomolecular processes and the underlying phenomena, thus, requires an accurate representation of the system's electrostatics. Computational methods like molecular dynamics simulations, owing to their atomistic resolution and the ability to describe biomolecular motion, interaction and structural fluctuations in atomic detail, have over time gained a lot of importance as a supporting tool for experiments in the quest to obtain mechanistic understanding of biological processes. With the important role that electrostatic interactions play in biology, accurate modelling of these interactions is important for obtaining reliable results from molecular simulations of biomolecules. In this review, we discuss the basics of biomolecular electrostatics, and state of the art and the recent developments in modelling electrostatic interaction in molecular dynamics simulations.

*Keywords:* Electrostatics, Biomolecules, Poisson-Boltzmann equation, MD Simulation, Particle Mesh Ewald.

**Article information:**
DOI: https://doi.org/10.71426/jasm.v1.i1.pp24-39
Received: *11 Nov. 2025* | Revised: *15 Dec. 2025* | Accepted: *27 Dec. 2025* | Published: *31 Dec. 2025*


## 1. Introduction

Electrostatic interaction plays a central role in many biological processes, ranging from storage of genetic information to binding partner recognition. Each $\mu$m sized cellular nucleus, for instance, holds 2 meters long DNA. The encasement of DNA within the nucleus requires very strong compaction of the negatively charged biopolymer with a very high linear charge density. The first level of this compaction is achieved by wrapping of the DNA around spherical cores consisting of positively charged histone proteins [1], giving rise to the nucleosome core particle [2], [3] (see figure 1(A)). Further compaction of the DNA into chromatin involves electrostatic interaction between the disordered N- and C-terminal regions of the core histones with the DNA of neighboring nucleosomes [4]. The decompaction of the compacted genetic material for the purpose of transcription also requires modulation of electrostatic interaction by the cellular transcription machinery through post-translational modifications [5]. In the sperm nuclei, during spermatogenesis, histone proteins are replaced by positively charged arginine-rich proteins called protamines (see Figure 1(B)), which bind the DNA major groove [6], [7] and utilize electrostatic interaction to compact the genetic material much more strongly in order to ascertain compact sperm head resulting in its smooth movement.

Electrostatic interaction is the most tunable and context-dependent interaction in proteins, making it one of the most powerful levers in protein engineering. Salt bridges can be introduced to stabilize certain folded conformations, while oppositely charged residues can be intentionally introduced at certain locations to destabilize certain conformations and promote conformational switching. Enzymes arrange charged residues so that the active site electric field stabilizes the transition state more than the ground state [8]. This is one of the strongest contributors to catalytic rate enhancement. Charged residues near the active site can be mutated to control transition-state stabilization [9], [10]. Electrostatic interaction affect the $pK_a$ of amino acid residues [11], [12], which can be utilized to engineer the activity pH of enzymes and design enzymes for non-native environments. Charged patches on protein surfaces determine protein-protein binding strength and specificity. Charge distribution on the surface can be modified to modulate binding strength, specificity and conformation.

Electrostatic interaction plays a vital role in determining the nature of interaction between antibodies in therapeutic

*Corresponding author
*Email address:* 525003@student.nitandhra.ac.in, sasisahasra.adari@gmail.com (Adari Sasi Sahasra), 525001@student.nitandhra.ac.in (Abdul Kowsar), arnab.mukherjee@qubit-pharmaceuticals.com (Arnab Mukherjee), sumsaur@gmail.com, sour000@gmail.com (Suman Saurabh).

**List of acronyms.**

| Acronym | Description |
|---|---|
| MD | Molecular Dynamics |
| PBE | Poisson–Boltzmann Equation |
| PB | Poisson–Boltzmann |
| GB | Generalized Born |
| PME | Particle Mesh Ewald |
| SPME | Smooth Particle Mesh Ewald |
| PPPM | Particle–Particle Particle–Mesh |
| FDM | Finite Difference Method |
| FEM | Finite Element Method |
| BEM | Boundary Element Method |
| PBC | Periodic Boundary Conditions |
| ff | Force Field |
| FFT | Fast Fourier Transform |
| APBS | Adaptive Poisson–Boltzmann Solver |
| QM/MM | Quantum Mechanics / Molecular Mechanics |
| CpHMD | Constant pH Molecular Dynamics |
| DNA | Deoxyribonucleic Acid |
| RNA | Ribonucleic Acid |
| mAb | Monoclonal Antibody |
| ARG | Arginine |
| Lys | Lysine |
| Asp | Aspartic Acid |
| Glu | Glutamic Acid |
| SPME | Smooth Particle Mesh Ewald |
| CHARMM | Chemistry at HARvard Macromolecular Mechanics |
| $pK_a$ | Acid Dissociation Constant |
| $\lambda_D$ | Debye Length |
| $\kappa$ | Debye Screening Parameter |

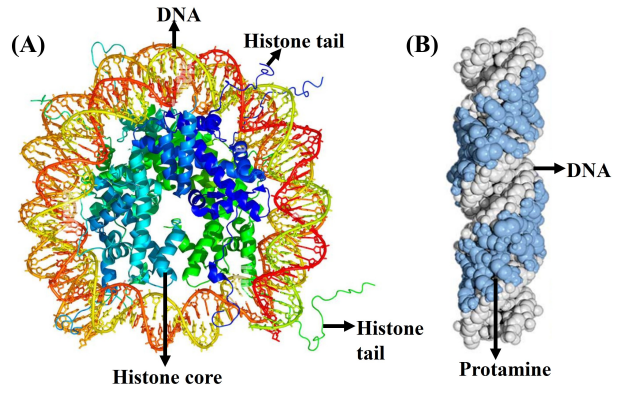


Figure 1: (Color online) (A) Structure of the nucleosome core particle showing negatively charged DNA wrapped around the positively charged histone core. The N- and C-terminal disordered regions of the histone proteins are also indicated. (B) Structure of the positively charged protamine bound within the major groove of a DNA molecule. Note: This illustration is adapted from [7].

solutions [13]. Certain therapeutic applications require high-concentration formulations leading to formation of protein aggregates. Such aggregated formulations have reduced therapeutic efficacy, and initiate an immune response when injected into the blood stream [14]. The interaction between the proteins is modulated by adding appropriate excipients and buffers into the formulation, which modify the inter-protein electrostatic interaction, however different species of excipients and buffers modify the interaction in different ways [13], [15]. The effect of these additional ions is complicated and depends on many factors like ionic concentration and the nature of the protein surface.

Interaction between two point charges in vacuum or in a dielectric medium is described by Coulomb's law ($F = \frac{1}{4\pi\varepsilon_0\varepsilon_r}\frac{q_1 q_2}{r^2}$), where $q_1$ and $q_2$ are the charges, $r$ is the distance between them, and $\varepsilon_0$ and $\varepsilon_r$ are the permittivity of free space and the relative dielectric constant of the medium, respectively.

Gauss' law states that the electric flux through a closed surface is proportional to the total charge enclosed within that surface. In differential form, it is written as (1):

$$\nabla \cdot \mathbf{E} = \frac{\rho(\mathbf{r})}{\varepsilon_0\varepsilon_r}, \tag{1}$$

In (1), $\mathbf{E}$ is the electric field and $\rho(\mathbf{r})$ is the charge density.

Since the electrostatic field is conservative, it can be expressed in terms of an electrostatic potential $\phi(\mathbf{r})$ as $\mathbf{E} = -\nabla\phi$.

Substituting this relation into Gauss' law yields Poisson's equation for the electrostatic potential in a medium of permittivity $\varepsilon = \varepsilon_0\varepsilon_r$ as (2), where $\rho(\mathbf{r})$ denotes the local charge density.

$$\nabla^2\phi(\mathbf{r}) = -\frac{\rho(\mathbf{r})}{\varepsilon}, \tag{2}$$

Dielectric media reduce the strength of electrostatic interaction between charges. The dielectric medium relevant to biomolecules is water. An aqueous medium in addition to modifying and screening inter-biomolecular interaction also plays the role of keeping the structure of the biomolecules intact. The overall structure of biomolecules originates from a balance between polar and non-polar interactions. Water, for instance, screens electrostatic repulsion between the backbones of the dsDNA strands and increases the clustering tendency of the hydrophobic bases attached to the strands resulting in the characteristic double-helical structure of the DNA molecule [16], [17]. The folded structure of the proteins originates from the tendency of hydrophobic amino acids to stay out of contact of water resulting in the formation of a hydrophobic core covered by charged and polar amino acids that have favorable interaction with water. In the cellular environment, in addition to water, biomolecules themselves form a part of the environment of other biomolecules and are assigned with their own dielectric constant. Protein, for instance, due to directional restraint of the constituent amino acids, is considered to have a low dielectric constant as compared to water [18]. Electrostatic screening is pronounced further by the presence of counter and co-ions. A charged molecule in water attracts counterions and repels co-ions. The overall ionic distribution around the charged molecules leads to the molecule presenting a lower (or higher) effective charge to other charged molecules in its surroundings [13].

Surface of biomolecules (especially proteins) do not have uniform distribution of charges but rather an inherent patchiness with regard to how the charge is distributed over the surface. Unevenly placed charged amino acids on the surface results in regions that are strongly charged

while the protein as a whole might be neutral. Such charge distributions give rise to strong local attraction or repulsion between proteins at close approach leading to directionality (anisotropy) of interaction, determining binding specificity, complex formation, and conformational stability. The heterogeneity of the surface charge and the irregular geometries of these biomolecules preclude determination of analytic solutions to the equations governing intermolecular electrostatics.

In recent times, molecular dynamics simulations and other computational methods have emerged as a very important supporting tool for experiments in understanding the mechanistic details of biological processes and in other application-based fields like drug discovery [19]. A proper treatment of the electrostatic interaction in simulations is necessary to sharpen the impact of such computational methods. In this review, we discuss the basics of biomolecular electrostatics, various numerical methods used to solve electrostatic equations and the methods used to evaluate electrostatic terms in explicit and implicit solvent simulations. We further discuss recent developments and future directions towards an accurate description and evaluation of electrostatic interaction in simulations.

## 2. Electrostatics in molecular dynamics simulations

Molecular dynamics simulation is a computational tool to obtain a trajectory of a molecule and its environment as a function of time. Ideas from statistical mechanics are then used to calculate various equilibrium and non-equilibrium properties of the system. To generate the trajectory, the initial positions and velocities $(r_i^0, v_i^0)$ of each particle constituting the system are used as an input. The total force on each particle that constitutes the system due to all other particles in the system is then calculated and then $(r_i^{\Delta t}, v_i^{\Delta t})$ at a future time $\Delta$t are evaluated by integrating the Newton's equations of motion. This process is repeated over multiple time steps $(t/\Delta t)$ and a complete trajectory over a time $t$ is generated. A *force field* (*ff*) is a mathematical model that describes the potential energy of a molecular system as a function of atomic coordinates. It consists of analytical expressions and associated parameters that approximate the interactions between atoms. These interactions are typically divided into *bonded* terms, which describe interactions between atoms connected by covalent bonds, and *non-bonded* terms, which describe interactions between atoms that are not directly bonded. *ff*s enable the calculation of forces (as derivatives of the potential energy function) acting on atoms, which are then used to propagate molecular dynamics trajectories.

The (3) represents various terms of the CHARMM *ff* [20] which is one of the most widely used *ff*s for proteins (other *ff*s use more or less similar potential functions):

$$\begin{aligned} U_{\text{CHARMM}} = & \sum_{\text{bonds}} k_b (r - r_0)^2 + \sum_{\text{angles}} k_\theta (\theta - \theta_0)^2 \\ & + \sum_{\text{Urey–Bradley}} k_{\text{UB}} (S - S_0)^2 \\ & + \sum_{\text{dihedrals}} k_\Phi \left[1 + \cos(n\Phi - \delta)\right] \\ & + \sum_{\text{impropers}} k_\omega (\omega - \omega_0)^2 \\ & + \sum_{i<j} \left[ \frac{A_{ij}}{r_{ij}^{12}} - \frac{B_{ij}}{r_{ij}^{6}} + \frac{q_i q_j}{4\pi\varepsilon_0 \varepsilon_r \, r_{ij}} \right]. \end{aligned} \tag{3}$$

The first five terms represent *bonded interactions*. The bond stretching term models deviations of the bond length $r$ from its equilibrium value $r_0$ using a harmonic potential with force constant $k_b$. The angle bending term describes deviations of the bond angle $\theta$ from its equilibrium value $\theta_0$, with force constant $k_\theta$. The Urey–Bradley term accounts for interactions between atoms separated by two bonds (1–3 interactions), where $S$ is the distance between the terminal atoms and $S_0$ its equilibrium value. The dihedral term describes torsional rotations around bonds, where $\Phi$ is the dihedral angle, $n$ is the multiplicity, $\delta$ is the phase shift, and $k_\Phi$ is the torsional force constant. The improper dihedral term enforces planarity or chirality, with $\omega$ representing the improper angle and $k_\omega$ its associated force constant. The final summation represents *non-bonded interactions*. The first two terms correspond to the Lennard–Jones potential, where the $r^{-12}$ term describes short-range Pauli repulsion and the $r^{-6}$ term describes attractive van der Waals dispersion (dipole-induced dipole) interactions. The last term is the Coulombic interaction between partial atomic charges $q_i$ and $q_j$ separated by distance $r_{ij}$, which constitutes the electrostatic part of the *ff*. Obtaining the contribution of the electrostatic interaction to the total potential energy of the system requires an accurate evaluation of this term.

## 3. Explicit and implicit solvent models

Biomolecules are usually studied in an aqueous environment, which is their native environment inside a cell. The accuracy of electrostatic calculations in biomolecular simulations depends on how realistically the solvent environment is represented. Since most biological processes occur in aqueous environments, the solvent plays a crucial role in screening electrostatic interactions, stabilising charged groups, and mediating biomolecular recognition. Two broad approaches are commonly used to model solvent effects: explicit solvent models and implicit solvent models. These approaches differ fundamentally in their treatment of electrostatics, physical realism, and computational efficiency.

In explicit solvent models, solvent molecules such as water and ions are represented as individual particles interacting through classical *ff*s. In the atomistic simulations, water molecules (and also solutes) are represented in atomic detail, using various water models [21]. In this approach the dielectric effect of water emerges automatically from pairwise electrostatic interactions of the atoms constituting the system. This approach captures molecular-level

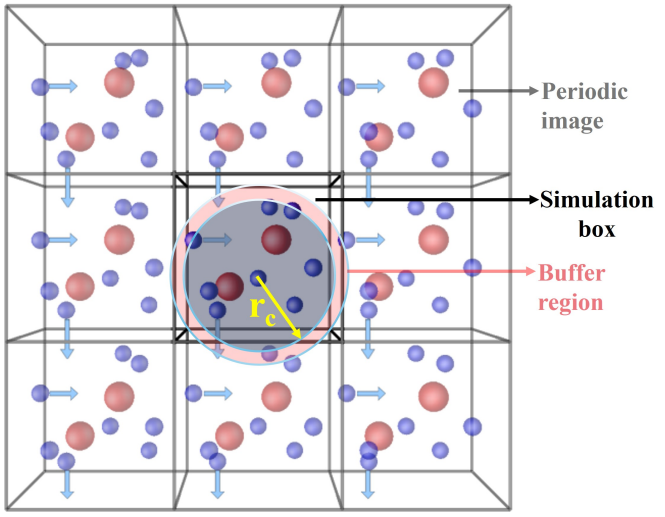


Figure 2: (Color online) The central box is a schematic representation of the simulation system. The surrounding boxes represent its periodic images. The blue sphere of radius $r_c$ (cut-off radius), centered at a reference particle, contains all neighboring particles contributing to its interactions. The red shell indicates the buffer region used to ensure accurate force calculations.

solvent structure, hydrogen bonding networks, hydration shells around biomolecules, and spatial variations in dielectric response. As a result, explicit solvent models provide a highly realistic description of biomolecular electrostatics. However, the inclusion of a large number of solvent molecules substantially increases the computational cost of simulations. In coarse-grained explicit solvent based simulations, an effective particle represents either one or a group of water molecules leading to a reduction in accuracy.

Implicit solvent models, in contrast, do not represent solvent molecules explicitly. Instead, the solvent is treated as a continuous medium characterised by an effective dielectric constant that mimics the average electrostatic screening effect of water. In this framework, biomolecules are embedded in a dielectric continuum, and electrostatic interactions are computed using continuum electrostatics theories rather than explicit solvent particles.

## 4. Electrostatics in explicit solvent setup

In explicit solvent MD simulations, periodic boundary conditions (PBC) are employed [22], wherein the finite sized simulation box that contains the system (solute + solvent) is replicated infinitely in all spatial directions (see Figure 2). This approach effectively mimics a bulk environment and mitigates finite-size and surface effects by allowing particles leaving one side of the box to re-enter from the opposite side. While PBC enable a more realistic representation of condensed-phase systems, they also render electrostatic interactions computationally demanding due to the long-range nature of Coulomb forces, which require specialized methods to efficiently account for interactions with periodic images.

### 4.1. Particle Mesh Ewald (PME)

In molecular simulations, the accurate treatment of Coulombic interactions is challenging because they are long-ranged and decay slowly with distance. Direct summation of pairwise electrostatic interactions in periodic systems is computationally prohibitive, while naïve truncation using cut-off distances can introduce significant artefacts. Ewald-based methods provide a systematic framework to overcome these limitations by enabling accurate and efficient computation of long-range electrostatics.

The classical Ewald summation method [22] decomposes the electrostatic energy of a periodic system into real-space and reciprocal-space contributions. For a system of charges $q_i$ at positions $\mathbf{r}_i$, the total electrostatic energy can be expressed as (4).

$$U = \frac{1}{2} \sum_{i \neq j} \frac{q_i q_j}{r_{ij}} \tag{4}$$

In (4), $r_{ij} = |\mathbf{r}_i - \mathbf{r}_j|$. In the Ewald formalism, this expression is rewritten as (5).

$$U = U_{\text{real}} + U_{\text{reciprocal}} + U_{\text{self}}, \tag{5}$$

In (5), $U_{\text{real}}$ represents short-range interactions computed in real space, $U_{\text{reciprocal}}$ accounts for long-range interactions evaluated in Fourier space, and $U_{\text{self}}$ is a correction term that removes spurious self-interactions. The real-space contribution is given by (6).

$$U_{\text{real}} = \frac{1}{2} \sum_{i \neq j} \frac{q_i q_j \operatorname{erfc}(\alpha r_{ij})}{r_{ij}} \tag{6}$$

In (6), $\alpha$ is the Ewald splitting parameter controlling the division between real and reciprocal space, and erfc is the complementary error function. The reciprocal-space contribution is written as (7).

$$U_{\text{reciprocal}} = \frac{1}{2V} \sum_{\mathbf{k} \neq 0} \frac{4\pi}{k^2} \exp\left(-\frac{k^2}{4\alpha^2}\right) \left| \sum_j q_j e^{i\mathbf{k}\cdot\mathbf{r}_j} \right|^2 \tag{7}$$

In (7), $V$ is the simulation cell volume and $\mathbf{k}$ are reciprocal lattice vectors.

Although the Ewald summation is highly accurate, its computational cost scales poorly with system size, motivating the development of more efficient mesh-based algorithms. The Particle Mesh Ewald (PME) [22] method accelerates the reciprocal-space calculation by interpolating particle charges onto a discrete mesh and evaluating the Fourier-space sums using Fast Fourier Transforms. This reduces the computational scaling to approximately $O(N \log N)$, enabling its application to large biomolecular systems. The long-range electrostatic potential $\phi(\mathbf{r})$ in PME is obtained by solving Poisson's equation on the mesh is expressed as (8).

$$\nabla^2 \phi(\mathbf{r}) = -\frac{\rho(\mathbf{r})}{\varepsilon_0} \tag{8}$$

In (8), $\rho(\mathbf{r})$ is the charge density mapped onto the grid. Higher-order interpolation schemes, such as B-spline functions, are employed to improve accuracy and reduce discretisation errors.

Closely related to PME is the Particle–Particle Particle–Mesh (PPPM) method [23], which also separates electrostatic interactions into short-range particle–particle and long-range mesh-based components. While PPPM was originally developed in plasma physics and soft-matter simulations, it has been adapted for molecular dynamics and shares conceptual similarities with PME, differing mainly in interpolation strategies and implementation details. Further refinements, such as Smooth Particle Mesh Ewald (SPME) [24] and multilevel Ewald approaches, have enhanced numerical stability, accuracy, and parallel scalability. By combining rigorous electrostatic theory with computational efficiency, these methods provide a reliable foundation for modelling biomolecular interactions in complex, solvated, and charged environments, thereby significantly improving the realism and predictive capability of molecular simulations.

### *4.2. Electrostatic cut-off Schemes*

While PME and related Ewald-based methods provide an accurate and efficient treatment of long-range electrostatics, their computational cost can still be significant for very large systems or long simulation times. Consequently, many molecular simulation studies also employ cut-off schemes to approximate electrostatic interactions. In these approaches, Coulombic interactions are evaluated explicitly only up to a finite distance, known as the cut-off radius $r_c$, beyond which interactions are neglected or treated approximately. Several cut-off strategies have been proposed to reduce artefacts associated with abrupt truncation of the Coulomb potential [25], [26], [27].

The simplest approach is the *hard cut-off* scheme, in which the electrostatic potential between two charges $q_i$ and $q_j$ is given by (9).

$$U_{ij}(r) = \begin{cases} \dfrac{q_i q_j}{4\pi\varepsilon_0 r}, & r \le r_c \\ 0, & r > r_c \end{cases} \tag{9}$$

In (9), $r$ is the interparticle distance and $\varepsilon_0$ is the vacuum permittivity. Although computationally efficient, this abrupt truncation leads to discontinuities in the potential and forces, often resulting in unphysical behaviour.

To mitigate these issues, *shifted potential* schemes modify the Coulomb interaction such that the potential smoothly approaches zero at the cut-off distance is given by (10).

$$U_{ij}^{\text{shift}}(r) = \frac{q_i q_j}{4\pi\varepsilon_0}\left(\frac{1}{r} - \frac{1}{r_c}\right), \quad r \le r_c \tag{10}$$

This ensures continuity of the potential at $r = r_c$, although the force may still exhibit discontinuities.

A more refined approach is the *switching function* method, in which the Coulomb potential is gradually damped within a switching region $r_s < r < r_c$ is expressed as (11).

$$U_{ij}^{\text{switch}}(r) = S(r)\,\frac{q_i q_j}{4\pi\varepsilon_0 r} \tag{11}$$

where $S(r)$ is a smooth switching function satisfying $S(r) = 1$ for $r \le r_s$ and $S(r) = 0$ for $r \ge r_c$. A commonly used polynomial switching function is follows (12).

$$S(r) = 1 - 10x^3 + 15x^4 - 6x^5, \quad x = \frac{r - r_s}{r_c - r_s}. \tag{12}$$

An alternative physically motivated scheme is the *reaction-field* method [28], which assumes that the region beyond the cut-off radius behaves as a dielectric continuum with permittivity $\varepsilon_{\text{rf}}$. The modified electrostatic potential is expressed as (13).

$$U_{ij}^{\text{RF}}(r) = \frac{q_i q_j}{4\pi\varepsilon_0 r}\left[1 + \frac{\varepsilon_{\text{rf}} - 1}{2\varepsilon_{\text{rf}} + 1}\left(\frac{r^3}{r_c^3} - 1\right)\right], \quad r \le r_c. \tag{13}$$

The reaction-field approach partially accounts for long-range electrostatic effects and is often used in simulations of condensed-phase systems.

The implementation of electrostatic cut-off schemes requires maintaining a neighbor list [22]. For a given atom, the neighbor list contains information about atoms that lie within the interaction range, defined by $r_c$ together with a small buffer region (see Figure 2). As solute and solvent molecules undergo diffusive motion during the simulation, the composition of the neighbor list evolves with time and therefore must be updated periodically. In atomistic molecular dynamics simulations, this update is typically performed every few to several time steps to balance computational efficiency and accuracy. If the neighbor list is not updated sufficiently frequently, new atoms may enter the interaction range between updates, which can introduce small errors in the evaluation of electrostatic interactions. Despite their computational efficiency, electrostatic cut-off schemes can introduce systematic errors in structural, dynamical, and thermodynamic properties, particularly in highly charged or heterogeneous biomolecular systems [**?** ], [30]. Therefore, modern molecular simulations frequently combine short-range cut-off treatments with PME, achieving a balance between computational efficiency and physical accuracy. A comparison between PME and cut-off schemes is provided in table 1.

## 5. Electrostatics in implicit solvent setup

One widely used implicit solvent approach is the Poisson–Boltzmann (PB) model. In the PB model, the electrostatic potential around a biomolecule is obtained by solving the Poisson–Boltzmann equation (PBE), which describes how electric fields and ionic distributions respond to fixed charges in a dielectric medium. This method accounts for the influence of solvent polarity and mobile ions in an averaged manner, providing a physically grounded description of electrostatic screening.

### *5.1. The Poisson–Boltzmann approach*

#### *5.1.1. The Poisson-Boltzman equation*

The Poisson-Boltzmann equation [31] describes the electrostatic potential arising from charged surfaces immersed in electrolytes [32]. Such a scenario is common for biomolecular systems [33] and in many other real-world applications such as semiconductor interfaces [34], electrodes in batteries and fuel cells etc [35]. The spatial distribution of ions near such surfaces determines electrostatic forces. In idealized models, charge density is often fixed and we determine the electrostatic potential of such surfaces from Poisson equation. However, in realistic physical systems, the ionic distribution depends both on the electrostatic

Table 1: Comparison of particle mesh Ewald (PME) and electrostatic cut-off schemes in molecular simulations.

| S. No. | Aspect | Particle Mesh Ewald (PME) | Electrostatic Cut-off Schemes |
|---|---|---|---|
| 1. | Treatment of long-range electrostatics | Explicitly evaluates long-range Coulomb interactions using reciprocal-space Fourier summation combined with real-space Ewald decomposition, ensuring full electrostatic representation under periodic boundary conditions. | Electrostatic interactions are truncated beyond a predefined cut-off radius, and contributions from distant particles are either ignored or approximated using shift or switch functions. |
| 2. | Computational scaling | Scales as $O(N \log N)$ due to the use of fast Fourier transform (FFT) algorithms for reciprocal-space computations. | Scales approximately as $O(N)$ when efficient neighbour list and domain decomposition techniques are employed. |
| 3. | Accuracy | High accuracy; considered the benchmark method for periodic systems. Accurately captures long-range electrostatic correlations, collective charge interactions, and periodic image effects. | Moderate to low accuracy; highly dependent on cut-off radius and smoothing method. Long-range electrostatic correlations are incompletely represented. |
| 4. | Continuity of potential and forces | Provides smooth, continuous, and differentiable electrostatic potential and forces across the simulation domain, ensuring numerical stability. | Hard cut-off methods introduce discontinuities in energy and force. Shifted or switched cut-offs improve continuity but remain approximate. |
| 5. | Physical realism | Accurately represents periodic boundary conditions and long-range Coulomb interactions, ensuring physically realistic electrostatic behaviour. | Limited physical realism due to neglect of long-range electrostatic contributions, especially in charged systems. |
| 6. | Typical applications | Widely used in atomistic simulations of biomolecules, proteins, nucleic acids, lipid membranes, ionic systems, and solvated macromolecules. | Commonly used in coarse-grained simulations, large-scale exploratory studies, and computationally constrained environments. |
| 7. | Sensitivity to parameters | Depends on mesh spacing, interpolation order, Ewald splitting parameter, and grid resolution. | Depends on cut-off radius, switching function, and neighbour list update parameters. |
| 8. | Computational cost | Higher computational cost due to FFT calculations and reciprocal-space operations. | Lower computational cost with reduced computational overhead. |
| 9. | Suitability for biomolecular simulations | Highly suitable and recommended for accurate atomistic biomolecular simulations. | Less suitable for high-precision biomolecular simulations; mainly used for approximate modelling. |

interaction and thermal agitations. Understanding this interplay is essential for describing equilibrium behavior in ionic systems.

The ions with a charge opposite to that of the surface are trapped very close to the surface resulting in the formation of a rigidly held ionic layer on the charged surface known as the *stern layer* [37]. Beyond the stern layer, the ions are loosely arranged and form a diffused layer with gradually decaying concentration. The stern and the diffused layer beyond it forms what is called the *ionic double layer* [38] (see Figure 3).

Considering a symmetric 1:1 electrolyte with bulk ionic number density $n_0$, the local number densities of positive and negative ions follow Boltzmann statistics and which is expressed as (14).

$$n_{\pm}(\mathbf{r}) = n_0 \exp\left(\mp \frac{e\phi(\mathbf{r})}{k_B T}\right). \tag{14}$$

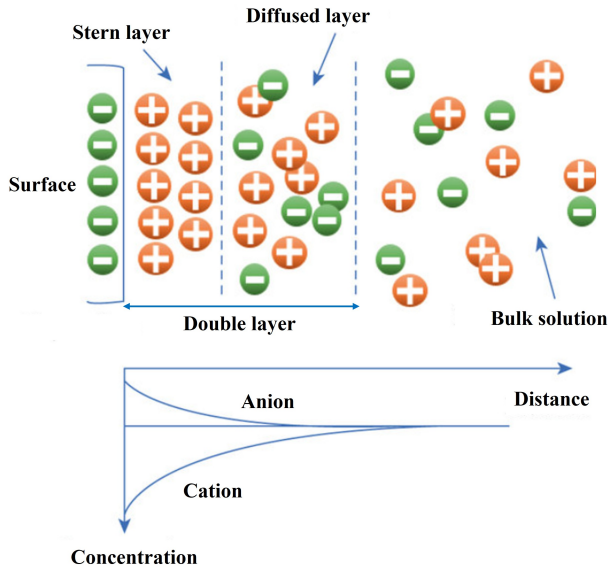


Figure 3: (Color online) Stern layer and electric double layer near a charged surface in an electrolyte medium, along with the variation of cation and anion concentrations as a function of distance from the surface. Note: This illustration is adapted from [36].

Therefore, the local charge density is follows (15).

$$\rho(\mathbf{r}) = e\left[n_+(\mathbf{r}) - n_-(\mathbf{r})\right] = -2en_0 \sinh\left(\frac{e\phi(\mathbf{r})}{k_B T}\right) \quad (15)$$

The total charge density is the sum of the free charge density and the local charge density in the solvent, i.e. $\rho_{tot}(r) = \rho(r) + \rho_f(r)$. Substituting $\rho_{tot}(r)$ into Poisson's equation yields PBE (16):

$$\nabla^2\phi(\mathbf{r}) = \frac{2en_0}{\varepsilon} \sinh\left(\frac{e\phi(\mathbf{r})}{k_B T}\right) - \frac{\rho_f(r)}{\varepsilon} \quad (16)$$

The (6) is nonlinear and generally does not admit analytical solutions. For weak electrostatic potentials satisfying $|e\phi/\mathrm{k}_B\mathrm{T}| \ll 1$, the hyperbolic sine function may be linearized, (as $\sinh x \approx x$) for $|x| \ll 1$. Applying this approximation gives the linearized PBE or the (D-H) equation (17) [39]:

$$\nabla^2\phi(\mathbf{r}) = \frac{2e^2n_0}{\epsilon k_B T}\phi(\mathbf{r}) - \frac{\rho_f(r)}{\varepsilon} \quad (17)$$

Defining $\kappa^2 = 2e^2n_0/\varepsilon k_B T$, the equation becomes: $\nabla^2\phi = \kappa^2\phi - \rho_f/\epsilon$, and $\kappa$ is referred to as the *Debye screening parameter* and quantifies the decay of electrostatic interactions due to ionic screening in the electrolyte.

For a point charge $q$ located at the origin, the governing equation is $\nabla^2\phi - \kappa^2\phi = -\frac{q}{\varepsilon}\delta(\mathbf{r})$, with the spherically symmetric solution: $\phi(r) = \frac{q}{4\pi\varepsilon r}e^{-\kappa r}$, which represents a screened Coulomb potential. The characteristic screening length is the *Debye length* $\lambda_D = \kappa^{-1}$. Electrostatic interactions decay exponentially beyond this length scale. For an electrolyte with ionic species $i$ of valency $z_i$ and bulk number density $n_i^\infty$, the screening parameter becomes (18):

$$\kappa^2 = \frac{e^2}{\varepsilon k_B T}\sum_i n_i^\infty z_i^2 \quad (18)$$

The D-H theory, thus, emerges as the linearized limit of the PBE, yielding a screened Coulomb interaction characterized by $\lambda_D$. PBE is widely used in biomolecular studies because it provides a physically grounded and computationally efficient description of electrostatic interactions in solvated biological systems. The PBE is a continuum electrostatics model in which the solvent is treated as a dielectric medium and mobile ions are described by statistical distributions, allowing the calculation of electrostatic potentials around proteins, nucleic acids, and other biomolecules without explicitly modelling individual solvent molecules [40], [41], [42]. This makes the PBE particularly suitable for predicting solvation energies [43], electrostatic potentials, and $pK_a$ shifts [44] in simulations of large biomolecular systems. However, the PBE has inherent limitations because it *neglects molecular-level solvent structure*, specific ion interactions, and dynamic fluctuations of water molecules. As a result, it cannot accurately describe processes that depend on explicit hydrogen bonding, ion coordination, or highly heterogeneous dielectric environments, such as membrane systems, strongly confined water, or short-range solvent-mediated interactions. The accuracy of PBE decreases for electrolytes containing multivalent or highly concentrated ions because its mean-field approximation neglects ion–ion correlations and finite ion size effects. Under such conditions, strong electrostatic coupling and specific ion interactions lead to deviations from the idealized Boltzmann distribution assumed in the model. Despite these limitations, the PBE remains a powerful and widely used tool for capturing long-range electrostatic effects in biomolecular modelling.

### *5.1.2. Boundary conditions and dielectric interfaces*

In continuum electrostatics models such as the PB framework, biomolecular systems are represented as regions with different dielectric properties. Typically, the biomolecule is assigned a low dielectric constant $\varepsilon_{\text{in}}$, while the surrounding solvent is assigned a higher dielectric constant $\varepsilon_{\text{out}}$ [18]. The surface separating these regions is known as a dielectric interface.

To obtain physically meaningful electrostatic potentials as solutions of the underlying differential equations, appropriate boundary conditions must be imposed at dielectric interfaces and at the outer boundaries of the computational domain. The electrostatic potential $\phi(\mathbf{r})$ is required to be continuous across the dielectric interface, which can be expressed as (17) [45]:

$$\phi_{\text{in}}(\mathbf{r}) = \phi_{\text{out}}(\mathbf{r}), \quad (19)$$

where $\phi_{\text{in}}$ and $\phi_{\text{out}}$ denote the electrostatic potentials inside and outside the biomolecule, respectively.

In addition, the normal component of the electric displacement field must be conserved across the interface. The electric displacement field $\mathbf{D}$ is defined as $\mathbf{D} = \varepsilon\nabla\phi$, and the corresponding boundary condition is given by (20) [45]:

$$\varepsilon_{\text{in}}\frac{\partial\phi_{\text{in}}}{\partial n} = \varepsilon_{\text{out}}\frac{\partial\phi_{\text{out}}}{\partial n}, \quad (20)$$

In (20), $\partial/\partial n$ denotes the derivative along the direction normal to the interface.

At the outer boundary of the simulation domain, far from the biomolecule, the electrostatic potential is typically assumed to vanish or approach a reference value. This condition is expressed as (21) [45]:

$$\phi(\mathbf{r}) \to 0 \quad \text{as} \quad |\mathbf{r}| \to \infty. \tag{21}$$

These boundary conditions ensure that the electrostatic potential and electric fields are physically consistent across regions of different dielectric properties. Accurate treatment of dielectric interfaces is crucial for reliable prediction of electrostatic potentials, solvation energies, and protonation equilibria in biomolecular systems.

### *5.1.3. Numerical Solution of PBE with Dielectric Discontinuities*

We will now look at the continuum electrostatic model of a solvated biomolecular system in which the solute region represents a protein of irregular shape containing a distribution of fixed atomic charges. The interior of the protein is characterized by a dielectric constant $\varepsilon_{\text{in}}$, reflecting its limited polarizability, while the surrounding solvent is modeled as an electrolyte continuum with dielectric constant $\varepsilon_{\text{out}}$ and mobile ions in thermal equilibrium. The interface between the solute and solvent is defined by the molecular surface separating these dielectric regions.

Let $\phi(\mathbf{r})$ denote the electrostatic potential at position $\mathbf{r}$. Within the solute region $\Omega_{\text{in}}$, the potential satisfies Poisson's equation (22).

$$-\nabla \cdot (\varepsilon_{\text{in}}(\mathbf{r})\nabla\phi(\mathbf{r})) = \sum_k q_k\, \delta(\mathbf{r} - \mathbf{r}_k), \qquad \mathbf{r} \in \Omega_{\text{in}} \tag{22}$$

In (22), $q_k$ and $\mathbf{r}_k$ denote the charge and position of the $k$-th atom, respectively, and $\varepsilon_{\text{in}}(\mathbf{r})$ allows for spatial variation of the dielectric constant within the protein.

In the solvent region $\Omega_{\text{out}}$, the electrostatic potential obeys the nonlinear PBE. The equation for a 1:1 electrolyte is expressed as (23).

$$-\varepsilon_{\text{out}}\, \nabla^2\phi(\mathbf{r}) \;+\; 2en_0\, \sinh\!\left(\frac{e\,\phi(\mathbf{r})}{k_B T}\right) = 0, \qquad \mathbf{r} \in \Omega_{\text{out}} \tag{23}$$

In the general case of an electrolyte with multiple ionic species is written as (24).

$$-\varepsilon_{\text{out}}\, \nabla^2\phi(\mathbf{r}) \;+\; \sum_i z_i e\, n_i^{\infty} \exp\!\left(-\frac{z_i e\,\phi(\mathbf{r})}{k_B T}\right) = 0, \mathbf{r} \in \Omega_{\text{out}} \tag{24}$$

In (24), $z_i$ is the valency of ionic species $i$, $n_i^{\infty}$ is its bulk number density. At the solute–solvent interface $\Gamma$, the $\phi(r)$ satisfies standard dielectric boundary conditions discussed in section 5.1.2, equations 19, 20 and 21.

The most widely used method for solving this nonlinear boundary value problem is the *finite difference method* (FDM) [46]. In FDM, the entire computational domain is discretized using a uniform Cartesian grid with spacing $h$. The electrostatic potential is represented only at discrete grid points, denoted by $\phi_{i,j,k} = \phi(x_i, y_j, z_k)$.

The dielectric constant is represented as a *spatially varying, piecewise constant function*,

$$\varepsilon(\mathbf{r}) = \begin{cases} \varepsilon_{\text{in}}, & \mathbf{r} \in \Omega_{\text{in}} \\ \varepsilon_{\text{out}}, & \mathbf{r} \in \Omega_{\text{out}} \end{cases} \tag{25}$$

In (25), $\varepsilon(\mathbf{r})$ assigns the solute or solvent dielectric constant to each grid point based on its location relative to the biomolecule.

The differential operator $-\nabla \cdot (\varepsilon\nabla\phi)$ is approximated using finite differences. At each grid point $(i, j, k)$, the operator is written in terms of the potentials at neighboring grid points along the three Cartesian directions (26):

$$-\sum_{\alpha=x,y,z} \frac{\varepsilon_{i+\frac{1}{2}\alpha}(\phi_{i+\alpha} - \phi_i) - \varepsilon_{i-\frac{1}{2}\alpha}(\phi_i - \phi_{i-\alpha})}{h^2} \tag{26}$$

In (26), $\alpha$ labels the Cartesian directions, $\phi_{i\pm\alpha}$ are potentials at neighboring grid points, $\varepsilon_{i\pm\frac{1}{2}\alpha}$ are dielectric constants evaluated at midpoints between grid points, and $h$ is the uniform grid spacing.

Applying this discretization to the full nonlinear PBE yields, at each grid point, a general nonlinear algebraic equation expressed as (27).

$$-\sum_{\alpha=x,y,z} \frac{\varepsilon_{i+\frac{1}{2}\alpha}(\phi_{i+\alpha} - \phi_i) - \varepsilon_{i-\frac{1}{2}\alpha}(\phi_i - \phi_{i-\alpha})}{h^2} + 2en_0 \sinh\!\left(\frac{e\phi_i}{k_B T}\right) = \rho_i, \tag{27}$$

In (27), $\rho_i$ is the charge density mapped onto the grid. $\rho_i$ at each grid point is obtained by spreading each atomic charge over nearby grid points so that the charge is represented smoothly on the grid. Note that the RHS is non-zero only in $\Omega_{in}$, while the second term of the LHS is present only when the grid lies in $\Omega_{out}$.

The resulting coupled nonlinear system is solved iteratively, typically using methods such as successive over-relaxation, multigrid techniques, or Newton-like schemes, until convergence of the electrostatic potential is achieved across the grid.

Once the electrostatic potential is obtained, the electrostatic solvation free energy is computed by evaluating the interaction between the fixed charges and the reaction potential is written as (28).

$$G_{\text{elec}}^{\text{PB}} = \frac{1}{2}\sum_j q_j\, \phi_{\text{react}}(\mathbf{r}_j), \tag{28}$$

In (28), $\phi_{\text{react}}$ is the solvent reaction field at the position of charge $q_j$. Here, the reaction potential $\phi_{\text{react}}$ represents the component of the electrostatic potential arising from solvent polarization and ionic screening, excluding the direct Coulomb potential of the fixed charges. In practice, it is obtained by subtracting the vacuum (or solute-only) electrostatic potential from the total solution of PBE.

In this formulation, the dielectric boundary conditions are enforced only approximately through grid-based averaging. Because of its conceptual simplicity, numerical robustness, and ease of implementation on regular grids, the finite difference method remains the most widely used approach for solving PBE and is employed in widely used PB solvers like APBS [47], [48] and DelPhi.

In addition to FDM, two other important numerical frameworks are often discussed: the *finite element method* (FEM) [49] and the *boundary element method* (BEM) [50].

Table 2: Comparison of explicit and implicit solvent models in biomolecular simulations with emphasis on electrostatic interactions.

| S. No. | Aspect | Explicit solvent models | Implicit solvent models |
|---|---|---|---|
| 1. | Representation of solvent | Solvent molecules and ions represented as discrete particles | Solvent represented as a continuous dielectric medium |
| 2. | Treatment of electrostatics | Direct computation, typically using PME or Ewald-based methods | Computed using continuum models such as PB or GB |
| 3. | Electrostatic screening | Emerges from molecular interactions of water and ions | Described by an effective dielectric constant |
| 4. | Solvent structure and H-bonding | Explicitly captured at atomic resolution | Not represented explicitly |
| 5. | Computational cost | High due to large number of solvent particles | Significantly lower |
| 6. | Accuracy of biomolecular interactions | High; suitable for detailed studies of protein–ligand binding, ion effects, and membrane systems | Moderate; suitable for qualitative trends |
| 7. | Time and length scales accessible | Limited by computational cost | Enables exploration of longer time scales and larger systems |
| 8. | Sensitivity | Dependent on *ff*, water model, and long-range electrostatics computation method | Dependent on dielectric constants and continuum model assumptions |

These methods are theoretically powerful and can provide highly accurate treatments of electrostatics, but they are generally used less frequently in routine biomolecular simulations because they are more complex to implement and computationally more demanding.

In FEM [49], PBE is rewritten in a weak or variational form. The computational domain is divided into many small elements, typically tetrahedra, and the electrostatic potential is approximated using local basis functions defined over these elements. This approach allows very flexible representation of complex molecular geometries and dielectric boundaries, and it can incorporate adaptive mesh refinement where higher resolution is needed. Despite these advantages, FEM is less commonly used in large-scale biomolecular workflows.

BEM [50] takes a different approach by reformulating the electrostatic problem entirely in terms of quantities defined on the interface between the solute and the solvent. Instead of discretizing the full three-dimensional volume, only the molecular surface is discretized. The effects of dielectric mismatch and ionic screening are incorporated through boundary integral equations that describe surface polarization charges. While this approach can provide accurate treatment of interface physics and reduces the dimensionality of the problem, solving the resulting nonlinear integral equations can be computationally intensive, which limits its widespread use.

### *5.2. Generalized Born method*

The Generalized Born (GB) model [52], [53] is a widely used approximation to the PB framework for estimating electrostatic solvation effects. Instead of solving the PB equation numerically, the GB method uses analytical formulas to estimate how the solvent screens electrostatic interactions, making it much faster computationally while still capturing the main physical effects.

In the GB model, the electrostatic part of the solvation free energy, which represents the energetic cost of transferring the molecule from vacuum into solvent, is written as (29).

$$\Delta G_{\text{elec}}^{\text{GB}} = -\frac{1}{2}\left(1-\frac{1}{\varepsilon}\right)\sum_{i,j}\frac{q_i q_j}{f_{ij}}, \tag{29}$$

In (29), $q_i$ and $q_j$ are the partial charges on atoms $i$ and $j$, and $\varepsilon$ is the dielectric constant of the solvent (for example, about 80 for water). The summation runs over all pairs of atoms in the molecule. The quantity $f_{ij}$ is an effective distance that accounts for the reduction of electrostatic interactions due to solvent screening. A commonly used expression for $f_{ij}$ is (30):

$$f_{ij} = \sqrt{r_{ij}^2 + \alpha_i \alpha_j \exp\left(-\frac{r_{ij}^2}{4\alpha_i \alpha_j}\right)}, \tag{30}$$

In (30). $r_{ij}$ is the distance between atoms $i$ and $j$, and $\alpha_i$ and $\alpha_j$ are the Born radii. The Born radius of an atom measures how buried it is inside the molecule: atoms deep inside are less exposed to solvent and therefore experience weaker screening, while atoms near the surface are more strongly screened.

In this model, the interior of the biomolecule is treated as a region with low dielectric constant, reflecting limited ability to polarize, while the surrounding solvent is treated as a high-dielectric continuum. In practice, the electrostatic contribution computed from the GB model is usually combined with an additional nonpolar term that accounts

for effects such as cavity formation and dispersion interactions between the solute and solvent.

The electrostatic solvation energy computed from the GB (or PB) model is added to the molecular mechanics energy to obtain the total potential energy of the system. During simulations, electrostatic component of the forces on atoms are calculated by taking the gradient of the GB energy with respect to atomic positions, which captures how changes in distances between atoms and their exposure to solvent affect electrostatic screening.

Although implicit solvent models offer substantial computational advantages and are useful for large-scale simulations and rapid energy evaluations, they lack explicit solvent structure and cannot capture specific solvent-mediated interactions, such as hydrogen bonding or ion coordination. Consequently, explicit solvent models are generally preferred for detailed studies of biomolecular interactions, whereas implicit solvent models are often employed for qualitative analyses, conformational sampling, and high-throughput screening. A comparison of the two models is presented in Table 2

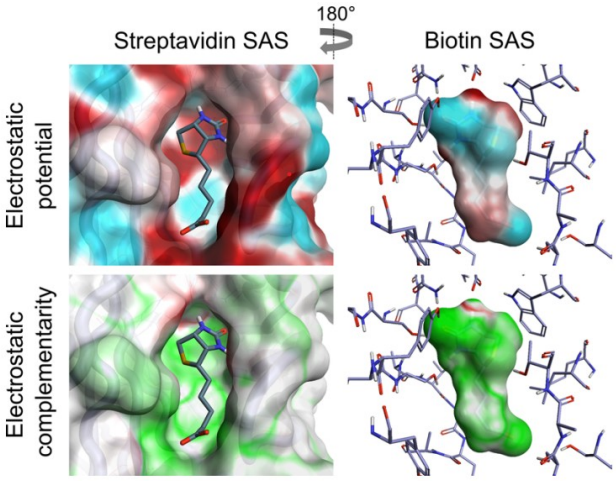


Figure 4: (Color online) (Top) Electrostatic potential color map of the solvent-accessible surface of the protein Streptavidin (left) and the ligand Biotin (right). Blue indicates negative electrostatic potential, while red indicates positive electrostatic potential. (Bottom) Electrostatic complementarity map showing complementary regions in green and electrostatic clashes in red for the protein (left) and ligand (right). The figure illustrates the electrostatic complementarity between the ligand and its binding pocket on the protein. Note: This illustration is adapted from [54].

## 6. Applications of electrostatic modelling in Biology

Electrostatic interactions play a central role in biological systems because most biomolecules contain charged or polar groups. In molecular simulations, electrostatic modelling refers to the computational description of interactions arising from electric charges and dipoles within and between biomolecules and their surrounding environment. Such interactions influence molecular recognition, stability, reactivity, and functional dynamics. Advances in electrostatic modelling, including Ewald-based methods and solvent representations, have therefore enabled deeper insights into a wide range of biological phenomena. Accurate modelling of electrostatics is important to increase the applicability of MD simulations and other predictive tools in assessing the molecular nature and energetics of protein–ligand binding, protein-protein and protein–surface interaction, enzyme catalysis, and drug docking conformations in protein binding pockets. In the following we discuss the importance of electrostatic interaction in the above mentioned phenomena.

### *6.1. Protein–ligand binding*

Protein–ligand binding refers to the process by which a small molecule (ligand) associates with a protein at a specific region known as the binding site. Electrostatic interactions contribute significantly to the binding affinity, which is the strength of the interaction between the protein and the ligand.

One important concept in this context is electrostatic complementarity [54] (see Figure 4). Electrostatic complementarity describes the matching of charge distributions between a protein and a ligand, such that regions of positive electric potential on one molecule align with regions of negative electric potential on the other. This complementarity enhances attractive Coulombic interactions, thereby stabilising the bound complex.

Another key contribution arises from salt bridges and hydrogen (H-) bonds. A salt bridge is an interaction between oppositely charged groups, typically involving a positively charged amino acid side chain (such as Lys or Arg) and a negatively charged side chain (such as Asp or Glu). H-bonds are directional interactions in which a H atom covalently bound to an electronegative atom (such as O or N) interacts with another electronegative atom. Both salt bridges and hydrogen bonds are largely governed by electrostatic forces and play a crucial role in determining the specificity and stability of protein–ligand complexes.

### *6.2. Protein–Protein and Protein–Surface interactions*

Electrostatic interactions play a central role in governing the stability, specificity, and kinetics of protein–protein interaction in biological and biomedical systems. These interactions depend on the distribution of charged and polar groups on protein surfaces and their coupling with the surrounding ionic environment. Electrostatic forces influence long-range attraction or repulsion, modulate binding affinities, and determine the orientation and accessibility of interacting biomolecules.

In protein–protein interactions, electrostatics contributes significantly to molecular recognition and binding. Proteins possess heterogeneous surface charge distributions resulting from ionisable amino acid residues such as Asp, Glu, Lys, Arg, and His. The net charge and local electrostatic potential of a protein depend strongly on pH and ionic strength. At long distances, electrostatic interactions guide proteins toward favorable orientations, while at short distances they

modulate binding free energies through salt bridges, hydrogen bonds, charge–dipole and cation$-\pi$ interactions.

A clinically relevant example is the interaction between therapeutic antibodies in solution [13]. Monoclonal antibodies (mAbs) are widely used in biopharmaceutical formulations, where their stability and aggregation behavior are strongly influenced by electrostatics. At a given pH, antibodies exhibit a characteristic net charge determined by their isoelectric point ($pI$). When the solution pH approaches the $pI$, electrostatic repulsion between antibody molecules is reduced, leading to enhanced attractive interactions and increased propensity for aggregation. Conversely, at pH values far from the $pI$, stronger electrostatic repulsion stabilizes the solution.

Ionic strength also plays a critical role in modulating antibody–antibody interaction. Increasing salt concentration typically screens electrostatic interactions. However, depending on the protein charge, electrostatic interaction between proteins can also be enhanced in the presence of multivalent ionic species [13] (see Figure 5). Multivalent ions can in some situations lead to protein aggregation by forming bridges between proteins that stabilize protein-protein dimers (see Figure 5). Understanding such phenomena is crucial in optimizing therapeutic antibody formulations to minimize aggregation while maintaining biological activity.

Protein adsorption onto solid surfaces is a fundamental process in biomedical devices, drug delivery systems, and biomaterials. Electrostatics often constitutes the dominant long-range interaction between proteins and surfaces, determining adsorption kinetics, orientation, and binding strength. The interaction depends on the surface charge density, protein charge distribution, and the ionic composition of the surrounding medium.

A prominent example is the interaction between antibodies and the silica surfaces of syringes used in pharmaceutical packaging. Silica surfaces typically bear negatively charged silanol groups at physiological pH. Antibodies, depending on their net charge and surface charge heterogeneity, can experience electrostatic attraction or repulsion when approaching silica surfaces. At pH values below the antibody's $pI$, antibodies carry a net positive charge and are electrostatically attracted to negatively charged silica, promoting adsorption. At higher pH values, electrostatic repulsion may reduce adsorption [51], owing to the change in sign of the protein charge and an increase in the negative charge of the silica surface, leading to repulsion. The repulsion may be specifically between certain regions of the antibodies (like the Fc fragment) and the surface, resulting in a change in adsorption conformation [51] (see Figure 6). Ionic strength further modulates these interactions by screening surface charges, thereby influencing the extent and reversibility of antibody adsorption. Such electrostatically driven adsorption can contribute to protein loss, denaturation, or aggregation in therapeutic formulations.

Electrostatics also plays a crucial role in the interaction between proteins and externally introduced glass-ceramic bone implants [55], [56], [57]. Glass ceramics release biologically relevant ions such as $Ca^{2+}$, $Na^{+}$, $SiO_4^{4-}$, and $PO_4^{3-}$ upon contact with physiological fluids [58]. Ion release modifies the local electrostatic environment and surface charge properties, thereby influencing protein adsorption and subsequent cellular responses. The formation of charged surface layers and ion-enriched interfacial regions alters the electrostatic potential landscape experienced by proteins. Local pH changes induced by ion exchange reactions at glass-ceramic surfaces further affect protein binding. These coupled effects of ion release and pH variation play a decisive role in determining the adsorption, orientation, and biological activity of proteins at implant surfaces, ultimately influencing processes such as osteointegration and tissue regeneration.

### *6.3. Enzyme catalysis*

Enzyme catalysis refers to the acceleration of chemical reactions by enzymes, which are biological macromolecules, usually proteins, that lower the activation energy required for a reaction to occur. Electrostatic interactions within the enzyme active site, which is the region where the substrate binds and the reaction takes place, are essential for catalytic efficiency.
Modelling the above mentioned phenomena in MD simulations requires accurate electrostatic parameters and calculations.

A major role of electrostatics in enzyme catalysis is the stabilization of transition states. The transition state is a high-energy, short-lived molecular configuration that occurs during the conversion of reactants into products. Electrostatic stabilization occurs when charged or polar groups in the enzyme active site interact favourably with the developing charges in the transition state, thereby lowering its energy [8], [59]. By reducing the energy barrier of the reaction, electrostatic stabilization significantly enhances reaction rates.

Computational electrostatic models, such as continuum electrostatics and explicit solvent simulations, allow the quantitative estimation of these stabilizing interactions and provide mechanistic insights into enzymatic function.

### *6.4. $pK_a$ predictions*

$pK_a$ is a measure of the tendency of an ionisable group to donate or accept a proton. In proteins, many amino acid side chains contain ionizable groups whose protonation states, meaning whether they are protonated (carrying a hydrogen ion) or deprotonated, depend on their local electrostatic environment.

Electrostatic modelling is widely used to predict $pK_a$ values of ionizable residues in biomolecules. One common approach involves calculating titration curves, which describe how the protonation state of a group changes as a function of pH. Titration curves are obtained by computing the free energy difference between protonated and deprotonated states under varying environmental conditions [60].

Electrostatics determines protonation states because the energy required to add or remove a proton depends on the local electric potential created by nearby charges, dipoles, and solvent molecules [61]. For example, a positively charged environment reduces the tendency of a group towards protonation, whereas a negatively charged environment stabilises the protonated form. By accurately modelling these electrostatic contributions, computational

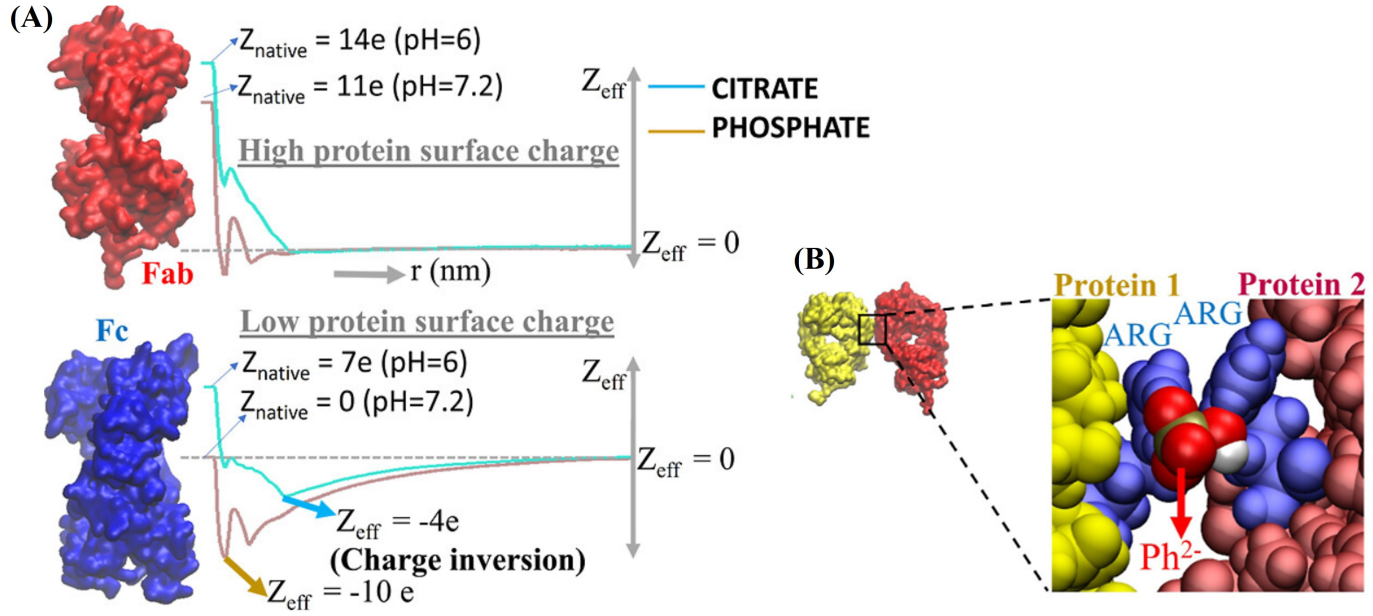


Figure 5: (Color online) (A) Effective charge as a function of distance for the Fab and Fc domains of antibody COE-3 with native charge $Z_{\text{native}}$, in the presence of phosphate and citrate ions at pH values of 6 and 7.2. The variation in effective charge highlights differences in the electrostatic environment surrounding highly charged (Fab) and weakly charged (Fc) domains. The effective charge of the Fab fragment approaches zero at short distances, indicating strong electrostatic screening. In contrast, the Fc fragment exhibits charge inversion under similar ionic conditions, which may result in inter-protein electrostatic repulsion. The effective charge at a given distance is computed by summing the intrinsic protein surface charge and the charges of all ions within that distance from the protein surface. (B) Molecular dynamics simulation snapshot showing a phosphate ion bridging two Fab fragments of antibody COE-3 by simultaneously binding to positively charged arginine (ARG) residues on both protein surfaces. Note: This illustration is adapted from [13].

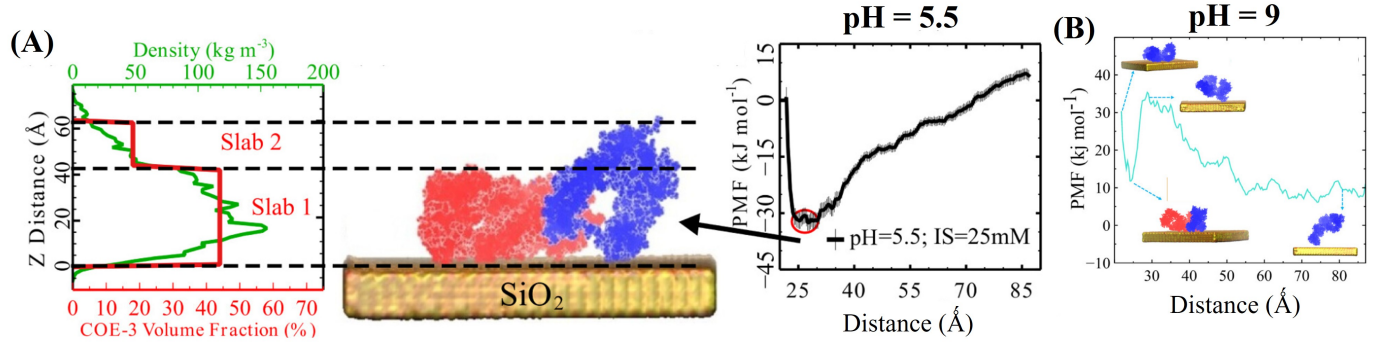


Figure 6: (Color online) (A) The middle panel shows the adsorbed conformation of antibody COE-3 on a silica surface at pH = 5.5, obtained from molecular dynamics simulations, representing the interaction of antibodies with glass storage container surfaces. The left panel shows neutron reflectivity data for COE-3 on silica at pH = 5.5 fitted using a slab model, providing experimental validation of the simulated binding conformation. The right panel presents the computed free energy profile as a function of the distance between the silica surface and the antibody, showing a deep minimum corresponding to the stable adsorbed conformation. (B) The free energy profile at pH = 9, with inset images showing significant changes in antibody–surface interaction and binding conformation. This conformational change is primarily electrostatic in origin. As pH increases from 5.5 to 9, the positive charge on the antibody decreases while the negative charge on the silica surface increases. Notably, the Fc domain (shown in blue) undergoes a charge transition from positive to negative. Note: This illustration is adapted from [51].

methods can predict shifts in $pK_a$ values relative to those observed in isolated amino acids in solution.

### *6.5. Drug design and docking*

Drug design refers to the rational development of small molecules that can modulate the function of biological targets, such as proteins or nucleic acids, in a predictable manner. Molecular docking is a computational technique used to predict the preferred binding orientation and binding strength of a ligand when it interacts with a target biomolecule. Electrostatic modelling plays a central role in both drug design and docking because electrostatic interactions strongly influence molecular recognition and binding energetics.

In molecular docking, the binding pose of a ligand is evaluated using scoring functions [62], [63], which are math-

ematical models that estimate the binding free energy of the protein–ligand complex. The binding free energy is the thermodynamic quantity that determines the stability of the bound state relative to the unbound state. Electrostatic contributions to the binding free energy arise from Coulombic interactions between charged groups, polarization effects, and solvent-mediated screening.

Electrostatic potentials of biomolecules are often computed to identify favourable regions for ligand binding. The electrostatic potential is a spatial map of the electric field generated by a biomolecule, which reflects the distribution of charges and dipoles. Regions of complementary electrostatic potential between a ligand and a protein are frequently associated with high binding affinity and specificity.

Furthermore, modelling and simulations are used to evaluate the influence of solvent and ionic strength on drug binding. Ionic strength refers to the concentration of ions in solution, which affects the screening of electrostatic interactions. By incorporating explicit or implicit solvent models, computational docking approaches can more accurately predict binding modes and affinities [64]. Consequently, electrostatic modelling has become an indispensable component of modern structure-based drug design.

## 7. Challenges and future directions

Despite significant advances in electrostatic modelling, several conceptual and computational challenges remain in accurately describing electrostatic interactions in biomolecular systems. These challenges arise from the inherent complexity of biological environments, the approximations used in theoretical models, and the trade-offs between computational efficiency and physical realism.

One major challenge is the ambiguity in assigning dielectric constants inside proteins. The dielectric constant is a measure of a material's ability to screen electric fields. In continuum electrostatics models, proteins are typically assigned a low dielectric constant to represent limited charge mobility, while solvent regions are assigned higher values. However, proteins exhibit heterogeneous internal environments, including polar, nonpolar, and flexible regions, making it difficult to define a single physically meaningful dielectric constant. This uncertainty can significantly influence calculated electrostatic potentials, solvation energies, and $pK_a$ values.

Another important limitation is the treatment of polarization effects. Polarization refers to the redistribution of electronic charge in response to an external electric field. Most conventional biomolecular *ff*s are non-polarizable, meaning that atomic charges are fixed and do not respond dynamically to their electrostatic environment. This approximation neglects many-body effects and limits the accuracy of electrostatic interactions, particularly in highly charged or heterogeneous environments. To address this limitation, polarizable *ff*s [65] have been developed. Examples include the AMOEBA *ff* [66], which incorporates atomic multipoles and induced dipoles, the Drude oscillator model [67], which represents electronic polarization using auxiliary particles attached to atoms, and the CHARMM polarizable *ff* [68], which extends classical CHARMM potentials to include explicit polarization effects. These approaches provide a more realistic description of electrostatics but at increased computational cost.

A further limitation of traditional molecular dynamics simulations is the treatment of protonation states as fixed quantities. In standard simulations, ionisable groups are assigned static protonation states based on predefined $pK_a$ values, ignoring the dynamic coupling between electrostatics and protonation. Constant-pH molecular dynamics (CpHMD) [69] simulations address this limitation by allowing protonation states of ionisable residues to change dynamically during the simulation in response to the local electrostatic environment and solution pH. In CpHMD, protonation equilibria are sampled alongside conformational dynamics, providing a more realistic representation of electrostatic effects in biological systems. Advanced implementations of CpHMD are available in major simulation packages such as AMBER [70], CHARMM [70], and GROMACS [71], and have been successfully applied to proteins, nucleic acids, and membrane systems.

Multiscale modelling approaches provide a framework for bridging different levels of physical description. A prominent example is the quantum mechanics/molecular mechanics (QM/MM) method, in which a chemically active region of a biomolecule is treated using quantum mechanics, while the surrounding environment is described classically. Quantum mechanics refers to a theory that explicitly describes electronic structure and chemical bonding, whereas molecular mechanics employs classical *ff*s to model atomic interactions. QM/MM methods enable accurate treatment of electronic effects in enzymatic reactions and charge transfer processes while maintaining computational feasibility. Widely used QM/MM frameworks include those implemented in software packages such as Gaussian [72], ORCA [73], CP2K [74], AMBER [75], and NAMD [76].

Recent developments in machine-learning-enhanced electrostatics offer new opportunities for improving both accuracy and efficiency. Machine learning refers to data-driven computational techniques that learn patterns from large datasets. In biomolecular electrostatics, machine learning models have been developed to predict atomic charges, electrostatic potentials, and interaction energies directly from molecular structures. Notable examples include neural network potentials, graph-based learning models, and deep learning frameworks integrated with molecular simulations. Tools such as DeepMD [77], ANI [78], SchNet [79], and equivariant neural networks have demonstrated promising performance in reproducing quantum-level electrostatic properties with significantly reduced computational cost.

In addition to these developments, several advanced computational tools have been created to improve the treatment of electrostatics in biomolecular systems. Examples include adaptive resolution simulation methods, which combine regions of different levels of resolution within a single simulation, enhanced sampling techniques such as metadynamics and replica-exchange molecular dynamics, which improve the exploration of electrostatically relevant conformational states, and hybrid continuum–atomistic models that couple PB solvers with MD simulations.

A persistent issue in electrostatic modelling is the trade-off between computational speed and physical accuracy.

Highly accurate methods, such as explicit solvent simulations with polarizable *ff*s, constant-pH dynamics, or quantum mechanical treatments, are computationally expensive, whereas faster methods, such as implicit solvent models or simplified electrostatic approximations, sacrifice molecular detail. Achieving an optimal balance between speed and accuracy remains a central challenge in computational biophysics.

## Declarations and Ethical Statements

***Conflict of Interest:*** The authors declare that there is no conflict of interest.

***Funding Statement:*** The authors declare that no specific funding was received for this research.

***Artificial Intelligence usage Statement:*** During the preparation of this manuscript, the authors utilized ChatGPT solely for language refinement and grammatical corrections. The authors carefully reviewed and revised the generated content and take full responsibility for the accuracy, integrity, and originality of the final manuscript.

***Availability of Data and Materials:*** The data and/or materials that support the findings of this study are available from the corresponding author upon reasonable request.

***Author Contribution Statement:***

Adari Sasi Sahasra and Abdul Kowsar (Equal contribution): Conducted the literature survey, performed data collection, and prepared the original draft of the manuscript.

Arnab Mukherjee: Contributed to formal analysis and developed the research methodology.

Suman Saurabh: Provided supervision, contributed to methodology development, prepared illustrations, and participated in manuscript drafting, review, and editing.

***Publisher's Note:*** The publisher of this article, Krrish Scientific Publications, remains neutral with regard to jurisdictional claims in published maps and institutional affiliations.

## References

[1] Estévez-Torres A, Baigl D. DNA compaction: fundamentals and applications. *Soft Matter*. 2011;7(15):6746-6756. Available from: https://doi.org/10.1039/C1SM05373F

[2] Davey CA, Sargent DF, Luger K, Maeder AW, Richmond TJ. Solvent mediated interactions in the structure of the nucleosome core particle at 1.9 resolution. *Journal of molecular biology*. 2002 Jun 21;319(5):1097-1113. Available from: https://doi.org/10.1016/S0022-2836(02)00386-8

[3] Onufriev AV, Schiessel H. The nucleosome: from structure to function through physics. *Current opinion in structural biology*. 2019 Jun 1;56:119-130. Available from: https://doi.org/10.1016/j.sbi.2018.11.003

[4] Saurabh S, Glaser MA, Lansac Y, Maiti PK. Atomistic Simulation of Stacked Nucleosome Core Particles: Tail Bridging, the H4 Tail, and Effect of Hydrophobic Forces. *The Journal of Physical Chemistry B* 2016 Mar 31;120(12):3048-3060. Available from: https://pubmed.ncbi.nlm.nih.gov/26931280/

[5] Semenyuk P, Muronetz V. Protein interaction with charged macromolecules: From model polymers to unfolded proteins and post-translational modifications. *International journal of molecular sciences*. 2019 Mar 12;20(5):1252. Available from: https://doi.org/10.3390/ijms20051252

[6] Mukherjee A, Saurabh S, Olive E, Jang YH, Lansac Y. Protamine binding site on DNA: molecular dynamics simulations and free energy calculations with full atomistic details. *The Journal of Physical Chemistry B*. 2021 Mar 23;125(12):3032-3044. Available from: https://pubs.acs.org/doi/10.1021/acs.jpcb.0c09166?goto=supporting-info

[7] Balhorn R. The protamine family of sperm nuclear proteins. Genome biology. 2007 Sep 26;8(9):227. Available from: https://doi.org/10.1186/gb-2007-8-9-227

[8] Bartlett GJ, Porter CT, Borkakoti N, Thornton JM. Analysis of catalytic residues in enzyme active sites. *Journal of molecular biology*. 2002 Nov 15;324(1):105-121 Available from: https://doi.org/10.1016/S0022-2836(02)01036-7

[9] Daubner SC, Fitzpatrick PF. Site-directed mutants of charged residues in the active site of tyrosine hydroxylase. *Biochemistry*. 1999 Apr 6;38(14):4448-4454. Available from: https://pubs.acs.org/doi/full/10.1021/bi983012u

[10] Russell AJ, Thomas PG, Fersht AR. Electrostatic effects on modification of charged groups in the active site cleft of subtilisin by protein engineering. *Journal of molecular biology*. 1987 Feb 20;193(4):803-813. Available from: https://doi.org/10.1016/0022-2836(87)90360-3

[11] Urry DW, Peng S, Parker T. Delineation of electrostatic-and hydrophobic-induced pka shifts in polypentapeptides: the glutamic acid residue. *Journal of the American Chemical Society*. 1993 Aug;115(16):7509-7510. Available from: https://pubs.acs.org/doi/pdf/10.1021/ja00069a063

[12] Davoodi J, Wakarchuk WW, Campbell RL, Carey PR, Surewicz WK. Abnormally High pKa of an Active-Site Glutamic Acid Residue in Bacillus Circulans Xylanase: The Role of Electrostatic Interactions. emphEuropean journal of biochemistry. 1995 Sep;232(3):839-843. Available from: https://doi.org/10.1111/j.1432-1033.1995.0839a.x

[13] Saurabh S, Zhang Q, Seddon JM, Lu JR, Kalonia C, Bresme F. Unraveling the microscopic mechanism of molecular ion interaction with monoclonal antibodies: impact on protein aggregation. *Molecular Pharmaceutics*. 2024 Feb 12;21(3):1285-1299. Available from: https://pubs.acs.org/doi/10.1021/acs.molpharmaceut.3c00963?goto=supporting-info

[14] Ren S. Current and emerging strategies for subcutaneous delivery of high-concentration and high-dose antibody therapeutics. *Journal of Pharmaceutical Sciences*. 2025 Aug 1;114(8):103877. Available from: https://doi.org/10.1016/j.xphs.2025.103877

[15] Saurabh S, Kalonia C, Li Z, Hollowell P, Waigh T, Li P, Webster J, Seddon JM, Lu JR, Bresme F. Understanding the stabilizing effect of histidine on mAb aggregation: a molecular dynamics study. *Molecular Pharmaceutics*. 2022 Aug 10;19(9):3288-3303. Available from: https://pubs.acs.org/doi/10.1021/acs.molpharmaceut.2c00453?goto=supporting-info

[16] Watson JD, Crick FH. The structure of DNA. In *Cold Spring Harbor symposia on quantitative biology*. 1953 Jan 1 (Vol. 18, pp. 123-131). Available from: https://symposium.cshlp.org/content/18/123.extract

[17] Alberts B, Johnson A, Lewis J, Raff M, Roberts K, Walter P. The structure and function of DNA. In *Molecular Biology of the Cell*. 4th edition 2002. Garland Science. Available from: https://www.ncbi.nlm.nih.gov/books/NBK26821/

[18] Schutz CN, Warshel A. What are the dielectric "constants" of proteins and how to validate electrostatic models?. *Proteins: Structure, Function, and Bioinformatics* 2001 Sep 1;44(4):400-417. Available from: https://doi.org/10.1002/prot.1106

[19] Saurabh S, Sivakumar PM, Perumal V, Khosravi A, Sugumaran A, Prabhawathi V. Molecular dynamics simulations in drug discovery and drug delivery. In *Integrative nanomedicine for new therapies*. 2020 Mar 3 (pp. 275-301). Cham: Springer International Publishing. Available from: https://doi.org/10.1007/978-3-030-36260-7_10

[20] Zhu X, Lopes PE, MacKerell Jr AD. Recent developments and applications of the CHARMM force fields. *Wiley Interdisciplinary Reviews: Computational Molecular Science*. 2012 Jan;2(1):167-185. Available from: https://doi.org/10.1002/wcms.74

[21] Kadaoluwa Pathirannahalage SP, Meftahi N, Elbourne A, Weiss AC, McConville CF, Padua A, Winkler DA, Costa Gomes M, Greaves TL, Le TC, Besford QA. Systematic comparison of the structural and dynamic properties of commonly used water models for molecular dynamics simulations. *Journal of Chemical Information and Modeling*. 2021 Aug 18;61(9):4521-4536. Available from: https://pubs.acs.org/doi/10.1021/acs.jcim.1c00794?goto=supporting-info

[22] Frenkel D, Smit B. Understanding molecular simulation: from algorithms to applications. *Elsevier*. 2023 Jul 13. Available from: https://doi.org/10.1016/B978-0-12-267351-1.X5000-7

[23] Luty BA, Davis ME, Tironi IG, Van Gunsteren WF. A comparison of particle-particle, particle-mesh and Ewald methods for calculating electrostatic interactions in periodic molecular systems. *Molecular Simulation*. 1994 Dec 1;14(1):11-20. Available from: https://doi.org/10.1080/08927029408022004

[24] Essmann U, Perera L, Berkowitz ML, Darden T, Lee H, Pedersen LG. A smooth particle mesh Ewald method. *The Journal of chemical physics*. 1995 Nov 15;103(19):8577-8593. Available from: https://doi.org/10.1063/1.470117

[25] Norberg J, Nilsson L. On the truncation of long-range electrostatic interactions in DNA. *Biophysical journal*. 2000 Sep 1;79(3):1537-1553. Available from: https://doi.org/10.1016/S0006-3495(00)76405-8

[26] Åqvist J, Hansson T. Analysis of electrostatic potential truncation schemes in simulations of polar solvents. *The Journal of Physical Chemistry B*. 1998 May 7;102(19):3837-3840. Available from: https://pubs.acs.org/doi/full/10.1021/jp973207w

[27] Loncharich RJ, Brooks BR. The effects of truncating long-range forces on protein dynamics. *Proteins: Structure, Function, and Bioinformatics*. 1989;6(1):32-45. Available from: https://doi.org/10.1002/prot.340060104

[28] Tironi IG, Sperb R, Smith PE, van Gunsteren WF. A generalized reaction field method for molecular dynamics simulations. *The Journal of chemical physics*. 1995 Apr 1;102(13):5451-5459. Available from: https://doi.org/10.1063/1.469273

[29] Bergdorf M, Peter C, Hünenberger PH. Influence of cut-off truncation and artificial periodicity of electrostatic interactions in molecular simulations of solvated ions: A continuum electrostatics study. *The Journal of chemical physics*. 2003 Nov 1;119(17):9129-9144. Available from: https://doi.org/10.1063/1.1614202

[30] Resat H, McCammon JA. Correcting for electrostatic cutoffs in free energy simulations: Toward consistency between simulations with different cutoffs. *The Journal of chemical physics*. 1998 Jun 15;108(23):9617-9123. Available from: https://doi.org/10.1063/1.476437

[31] Fogolari F, Brigo A, Molinari H. The Poisson–Boltzmann equation for biomolecular electrostatics: a tool for structural biology. *Journal of Molecular Recognition*. 2002 Nov;15(6):377-392. Available from: https://doi.org/10.1002/jmr.577

[32] Lamm G. The poisson–boltzmann equation. *Reviews in computational chemistry* 2003 Oct 3;19:147-365. Available from: https://doi.org/10.1002/0471466638.ch4

[33] Matsarskaia O, Roosen-Runge F, Schreiber F. Multivalent ions and biomolecules: Attempting a comprehensive perspective. *ChemPhysChem*. 2020 Aug 18;21(16):1742-1767. Available from: https://doi.org/10.1002/cphc.202000162

[34] Sparnaay MJ. On the electrostatic contribution to the interfacial tension of semiconductor/gas and semiconductor/electrolyte interfaces. *Surface Science*. 1964 Jul 1;1(3):213-224. Available from: https://doi.org/10.1016/0039-6028(64)90028-7

[35] Wu Y, Hu Q, Liang H, Wang A, Xu H, Wang L, He X. Electrostatic potential as solvent descriptor to enable rational electrolyte design for lithium batteries. *Advanced Energy Materials*. 2023 Jun;13(22):2300259. Available from: https://doi.org/10.1002/aenm.202300259

[36] Wan Y, Guo D, Hui X, Liu L, Yao Y. Studies on Hydration Swelling and Bound Water Type of Sodium-and Polymer-Modified Calcium Bentonite. Advances in Polymer Technology. 2020;2020(1):9361795. Available from: https://doi.org/10.1155/2020/9361795

[37] Brown MA, Goel A, Abbas Z. Effect of electrolyte concentration on the stern layer thickness at a charged interface. *Angewandte Chemie*. 2016 Mar 7;128(11):3854-3858. Available from: https://doi.org/10.1002/ange.201512025

[38] Mangelsdorf CS, White LR. The dynamic double layer Part 1Theory of a mobile Stern layer. *Journal of the Chemical Society, Faraday Transactions*. 1998;94(16):2441-2452. Available from: https://doi.org/10.1039/A803588A

[39] Hartley GS. The application of the Debye-Hückel theory to colloidal electrolytes. *Transactions of the Faraday Society*. 1935;31:31-50. Available from: https://pubs.rsc.org/en/content/articlelanding/1935/tf/tf9353100031/unauth

[40] Fogolari F, Brigo A, Molinari H. The Poisson–Boltzmann equation for biomolecular electrostatics: a tool for structural biology. *Journal of Molecular Recognition*. 2002 Nov;15(6):377-392. Available from: https://doi.org/10.1002/jmr.577

[41] Baker NA. Poisson–Boltzmann methods for biomolecular electrostatics. In *Methods in enzymology ,Academic Press*. 2004 Jan 1 (Vol. 383, pp. 94-118). Available from: https://doi.org/10.1016/S0076-6879(04)83005-2

[42] de Souza Gama M, Santos MS, de Almeida Lima ER, Tavares FW, Barreto Jr AG. A modified Poisson-Boltzmann equation applied to protein adsorption. *Journal of Chromatography A*. 2018 Jan 5;1531:74-82. Available from: https://doi.org/10.1016/j.chroma.2017.11.022

[43] Li B. Minimization of electrostatic free energy and the Poisson–Boltzmann equation for molecular solvation with implicit solvent. *SIAM Journal on Mathematical Analysis*. 2009;40(6):2536-2566. Available from: https://doi.org/10.1137/080712350

[44] Hu J, Zhao S, Geng W. Accurate pKa computation using matched interface and boundary (MIB) method based Poisson-Boltzmann solver. *Commun. Comput. Phys.* 2018 Feb 1;23(2):520-539. Available from: https://s2.smu.edu/wgeng/research/Hu_CiCP_2018.pdf

[45] Griffiths DJ. Introduction to electrodynamics. *Cambridge University Press*. 2023 Nov 2. Available from: https://www.cambridge.org/highereducation/books/introduction-to-electrodynamics/3AB220820DBB628E5A43D52C4B011ED4

[46] Sharp K. Incorporating solvent and ion screening into molecular dynamics using the finite-difference Poisson–Boltzmann method. *Journal of computational chemistry*. 1991 May;12(4):454-468. Available from: https://doi.org/10.1002/jcc.540120407

[47] Baker NA, Sept D, Joseph S, Holst MJ, McCammon JA. Electrostatics of nanosystems: application to microtubules and the ribosome. *Proceedings of the National Academy of Sciences*. 2001 Aug 28;98(18):10037-10041. Available from: https://doi.org/10.1073/pnas.181342398

[48] Jurrus E, Engel D, Star K, Monson K, Brandi J, Felberg LE, Brookes DH, Wilson L, Chen J, Liles K, Chun M. Improvements to the APBS biomolecular solvation software suite. *Protein science*. 2018 Jan;27(1):112-128. Available from: https://doi.org/10.1002/pro.3280

[49] Dhatt G, Lefrançois E, Touzot G. Finite element method. *John Wiley Sons*. 2012 Dec 27. Available from: https://onlinelibrary.wiley.com/doi/book/10.1002/9781118569764

[50] Boschitsch AH, Fenley MO, Zhou HX. Fast boundary element method for the linear Poisson Boltzmann equation. *The Journal of Physical Chemistry B*. 2002 Mar 14;106(10):2741-2754. Available from: https://pubs.acs.org/doi/full/10.1021/jp013607q

[51] Li Z, Saurabh S, Hollowell P, Kalonia CK, Waigh TA, Li P, Webster JR, Seddon JM, Bresme F, Lu JR. pH-Dependent Conformational Plasticity of Monoclonal Antibodies at the SiO2/Water Interface: Insights from Neutron Reflectivity and Molecular Dynamics. *ACS Applied Materials & Interfaces*. 2024 Dec 12;16(51):70231-70241. Available from: https://pubs.acs.org/doi/10.1021/acsami.4c14407

[52] Onufriev AV, Case DA. Generalized born implicit solvent models for biomolecules. *Annual review of biophysics*. 2019 May 6;48(1):275-296. Available from: https://doi.org/10.1146/an

nurev-biophys-052118-115325

[53] Bashford D, Case DA. Generalized born models of macromolecular solvation effects. *Annual review of physical chemistry*. 2000 Oct;51(1):129-152. Available from: https://doi.org/10.1146/annurev.physchem.51.1.129

[54] Bauer MR, Mackey MD. Electrostatic complementarity as a fast and effective tool to optimize binding and selectivity of protein–ligand complexes. *Journal of medicinal chemistry*. 2019 Feb 26;62(6):3036-3050. Available from: https://pubs.acs.org/doi/full/10.1021/acs.jmedchem.8b01925

[55] Tilocca A. Structural models of bioactive glasses from molecular dynamics simulations. *Proceedings of the Royal Society A: Mathematical, Physical and Engineering Sciences*. 2009 Apr 1;465(2104):1003-27. Available from: https://doi.org/10.1098/rspa.2008.0462

[56] Gruian C, Vanea E, Steinhoff HJ, Simon S. Glass-ceramics: fundamental aspects regarding the interaction with proteins. *Handbook of Bioceramics and Biocomposites*. 2016:667-701. Available from: https://doi.org/10.1007/978-3-319-09230-0_20-1

[57] Rosengren Å, Oscarsson S, Mazzocchi M, Krajewski A, Ravaglioli A. Protein adsorption onto two bioactive glass-ceramics. *Biomaterials*. 2003 Jan 1;24(1):147-155 Available from: https://doi.org/10.1016/S0142-9612(02)00272-7

[58] Verné E, Bretcanu O, Balagna C, Bianchi CL, Cannas M, Gatti S, Vitale-Brovarone C. Early stage reactivity and in vitro behavior of silica-based bioactive glasses and glass-ceramics. *Journal of Materials Science: Materials in Medicine*. 2009 Jan;20(1):75-87. Available from: https://doi.org/10.1007/s10856-008-3537-8

[59] Szefczyk B, Mulholland AJ, Ranaghan KE, Sokalski WA. Differential transition-state stabilization in enzyme catalysis: quantum chemical analysis of interactions in the chorismate mutase reaction and prediction of the optimal catalytic field. *Journal of the American Chemical Society*. 2004 Dec 15;126(49):16148-16159. Available from: https://pubs.acs.org/doi/full/10.1021/ja049376t

[60] Søndergaard CR, Olsson MH, Rostkowski M, Jensen JH. Improved treatment of ligands and coupling effects in empirical calculation and rationalization of p K a values. *Journal of chemical theory and computation*. 2011 Jul 12;7(7):2284-3395. Available from: https://pubs.acs.org/doi/full/10.1021/ct200133y

[61] Olsson MH. Protein electrostatics and pKa blind predictions; contribution from empirical predictions of internal ionizable residues *Proteins: Structure, Function, and Bioinformatics*. 2011 Dec;79(12):3333-3345. Available from: https://doi.org/10.1002/prot.23113Digital

[62] Pierce BG, Wiehe K, Hwang H, Kim BH, Vreven T, Weng Z. ZDOCK server: interactive docking prediction of protein–protein complexes and symmetric multimers *Bioinformatics*. 2014 Jun 15;30(12):1771-1773. Available from: https://doi.org/10.1093/bioinformatics/btu097

[63] Cosconati S, Forli S, Perryman AL, Harris R, Goodsell DS, Olson AJ. Virtual screening with AutoDock: theory and practice. *Expert opinion on drug discovery*. 2010 Jun 1;5(6):597-607. Available from: https://doi.org/10.1517/17460441.2010.484460

[64] Hou T, Wang J, Li Y, Wang W. Assessing the performance of the molecular mechanics/Poisson Boltzmann surface area and molecular mechanics/generalized Born surface area methods. II. The accuracy of ranking poses generated from docking. *Journal of computational chemistry*. 2011 Apr 15;32(5):866-877. Available from: https://doi.org/10.1002/jcc.21666

[65] Jing Z, Liu C, Cheng SY, Qi R, Walker BD, Piquemal JP, Ren P. Polarizable force fields for biomolecular simulations: Recent advances and applications. *Annual Review of biophysics*. 2019 May 6;48(1):371-394. Available from: https://doi.org/10.1146/annurev-biophys-070317-033349

[66] Mauger N, Plé T, Lagardère L, Huppert S, Piquemal JP. The Q-AMOEBA (CF) Polarizable Potential. *The Journal of Physical Chemistry Letters*. 2025 Jun 2;16(23):5723-31. Available from: https://pubs.acs.org/doi/full/10.1021/acs.jpclett.5c00797

[67] Lemkul JA, Huang J, Roux B, MacKerell Jr AD. An empirical polarizable force field based on the classical drude oscillator model: development history and recent applications. *Chemical reviews*. 2016 May 11;116(9):4983-5013. Available from: https://pubs.acs.org/doi/full/10.1021/acs.chemrev.5b00505

[68] Vanommeslaeghe K, MacKerell Jr AD. CHARMM additive and polarizable force fields for biophysics and computer-aided drug design. *Biochimica et Biophysica Acta (BBA)-General Subjects*. 2015 May 1;1850(5):861-871. Available from: https://doi.org/10.1016/j.bbagen.2014.08.004

[69] de Oliveira VM, Liu R, Shen J. Constant pH molecular dynamics simulations: Current status and recent applications. *Current opinion in structural biology*. 2022 Dec 1;77:102498. Available from: https://doi.org/10.1016/j.sbi.2022.102498

[70] Henderson JA, Liu R, Harris JA, Huang Y, de Oliveira VM, Shen J. A guide to the continuous constant pH molecular dynamics methods in Amber and CHARMM [Article v1. 0]. *Living journal of computational molecular science*. 2022 Aug 22;4(1):1563. Available from: https://doi.org/10.33011/livecoms.4.1.1563

[71] Aho N, Buslaev P, Jansen A, Bauer P, Groenhof G, Hess B. Scalable constant pH molecular dynamics in GROMACS. *Journal of Chemical Theory and Computation*. 2022 Sep 21;18(10):6148-6160. Available from: https://pubs.acs.org/doi/full/10.1021/acs.jctc.2c00516

[72] Demichelis R, Noel Y, D'Arco P, Rérat M, Zicovich-Wilson CM, Dovesi R. Properties of carbon nanotubes: an ab initio study using large gaussian basis sets and various dft functionals *The Journal of Physical Chemistry C*. 2011 May 12;115(18):8876-85. Available from: https://pubs.acs.org/doi/10.1021/jp110704x

[73] Neese F. The ORCA program system. *Wiley Interdisciplinary Reviews: Computational Molecular Science*. 2012 Jan;2(1):73-8. Available from: https://doi.org/10.1002/wcms.81

[74] Hutter J, Iannuzzi M, Schiffmann F, VandeVondele J. cp2k: atomistic simulations of condensed matter systems. *Wiley Interdisciplinary Reviews: Computational Molecular Science*. 2014 Jan;4(1):15-25. Available from: https://doi.org/10.1002/wcms.1159

[75] Götz AW, Clark MA, Walker RC. An extensible interface for QM/MM molecular dynamics simulations with AMBER. *Journal of computational chemistry*. 2014 Jan 15;35(2):95-108. Available from: https://doi.org/10.1002/jcc.23444

[76] Melo MC, Bernardi RC, Rudack T, Scheurer M, Riplinger C, Phillips JC, Maia JD, Rocha GB, Ribeiro JV, Stone JE, Neese F. NAMD goes quantum: an integrative suite for hybrid simulations. *Nature methods*. 2018 May 1;15(5):351-354. Available from: https://doi.org/10.1038/nmeth.4638

[77] Zeng J, Zhang D, Lu D, Mo P, Li Z, Chen Y, Rynik M, Huang LA, Li Z, Shi S, Wang Y. DeePMD-kit v2: A software package for deep potential models. *The Journal of Chemical Physics*. 2023 Aug 7;159(5). Available from: https://doi.org/10.1063/5.0155600

[78] Xue J, Terrel N, Pickering I, Roitberg A. LAMMPS-ANI: Large Scale Molecular Dynamics Simulations with ANI Neural Network Potential. *chemrxiv.org*. Available from: https://doi.org/10.26434/chemrxiv-2025-8v03m

[79] Schütt KT, Sauceda HE, Kindermans PJ, Tkatchenko A, Müller KR. Schnet–a deep learning architecture for molecules and materials. *The Journal of chemical physics*. 2018 Jun 28;148(24). Available from: https://doi.org/10.1063/1.5019779